Drop Deformation in Stokes Flow through Converging Channels

Luiz C. Wrobel[1*], Delfim Soares Jr[2] and Claire L. Das Bhaumik[1,3]

[1]School of Engineering and Design, Brunel University, Uxbridge UB8 3PH, UK

[2] Structural Engineering Department, Federal University of Juiz de Fora, Juiz de Fora, Brazil

[3]Current address: BRE, Garston, Watford WD25 9XX, UK

Keywords: Boundary elements, Stokes flow, drop deformation, drop interaction, converging channels

Abstract. This work presents an application of a direct BEM formulation for drop deformation and interaction in Stokes flows through converging channels. Parametric studies are conducted to investigate the effect, on drop deformation, of the channel's convergence ratio, the drop-fluid viscosity ratio, the interfacial tension and the initial relative position of the drops.

1. Introduction

Suspensions of particles, drops and bubbles in viscous fluids occur in many biological systems, industrial applications and processes including blood flow, pharmaceutical manufacturing, food and chemical processing. It is important to understand the properties of the suspensions in order to gain a better understanding of their behaviour in these systems. This knowledge can then be used to predict fluid behaviour and improve industrial processes.

The study of the motion of particles, drops and bubbles in viscous fluids at low Reynolds number dates back to 1851, when Stokes [1] published a paper on the problem of a rigid sphere translating through a fluid at zero Reynolds number. Since then, there has been much research in this area, both experimental and theoretical. Important areas

* Corresponding author. E-mail: luiz.wrobel@brunel.ac.uk; Tel: +44 1895 266696; Fax: +44 1895 269803.

of study include flow with rigid boundaries, such as solid inclusions and plane walls, and flows involving deformable boundaries, *e.g.* flows containing viscous liquid drops or gas bubbles [2].

The BEM is an efficient technique for problems involving deforming boundaries such as fluid-fluid interfaces. In these problems, the position of the interfaces must be determined as part of the solution. The BEM enables direct calculation of the interface velocity. Numerical techniques for ordinary differential equations can then be used to find new nodal positions. The BEM also has the ability to deal with large surface deformations and other surface effects, such as interfacial tension, can be easily incorporated [3, 4].

Recent reviews of boundary integral methods for viscous free-boundary problems involving the deformation of single and multiple fluid-fluid interfaces were produced by Weinbaum and Ganatos [5] and Tanzosh *et al*. [6], while a review of drop deformation and break-up at low Reynolds number flows was produced by Stone [7]. Briscoe *et al*. [8] reviewed developments in the understanding of the mixing process of a dispersed fluid phase in a continuous fluid phase.

Manga and Stone [9] used a boundary integral method to study the buoyancy-driven interactions between two deformable viscous drops based on a formulation similar to Rallison and Acrivos' pioneering work [10]. In this case large deformations are seen due to buoyancy forces being much larger than the restoring interfacial tension forces. The same formulation was later used to investigate the low Reynolds number motion of bubbles, drops and rigid spheres through fluid-fluid interfaces [11]. In this study, one of the drops was considered to be infinitely large. Manga and Stone [12] also carried out a three-dimensional study of the behaviour of deformable buoyant drops and bubbles in dilute low Reynolds number suspension, in which a boundary integral method was used to model up to four drops.

Pozrikidis [13] studied the buoyancy-driven motion of a train of drops in a vertical tube, with drops of the same viscosity as the surrounding fluid which settle or rise along the axis of a vertical cylindrical tube. The method employed used an axisymmetric periodic Green's function for flow in a cylindrical tube. Drop motion was studied as a function

of the tube radius σ_c, the drop radius *a,* the drop separation *L* and the Bond number. Two types of drops were considered, classified according to the value of the ratio σ_c/a. Drops where $\sigma_c/a>1$ were called compact drops, otherwise drops were called elongated. Where surface tension was large, compact drops assume a spherical shape and elongated drops tend to adhere to the tube wall. For compact drops, a smaller value of drop separation ratio *L/a* leads to more elongated drops and the drops develop a fishtail shape at the rear.

Zhou and Pozrikidis studied the two-dimensional flow of single files of drops [14] and the shear-driven flow of ordered periodic suspensions of two-dimensional liquid drops in a channel [15], using the method of interfacial dynamics. Periodically random suspensions were also studied. The behaviour of random suspensions was found to be significantly different from that of ordered suspensions.

Li *et al.* [16] studied the shearing motion of monodisperse suspensions of two-dimensional deformable liquid drops with uniform surface tension in an infinite domain. The drop viscosity was the same as that of the surrounding fluid. A periodic distribution of squares of randomly distributed drops was used. Loewenberger and Hinch [17] developed a three-dimensional numerical formulation for a concentrated emulsion in shear flow. As in the study of Li *et al.* [16], a periodic distribution of squares of randomly distributed drops is used. The number of random particles in each periodic box was limited to twelve due to computational costs. The emulsion was found to have complex non-Newtonian rheology.

Roumeliotis and Fulford [18] developed a boundary integral method in which the drop surfaces are parameterized with respect to arc length using cubic splines, enabling the surface tension to be represented as piecewise linear. This is applied to the buoyancy-driven interaction of two and three axisymmetric drops in Stokes flow.

In order to calculate the surface tension forces accurately, the surface curvature must be computed accurately. Zinchenko *et al.* [19] eliminated the mean curvature term from the boundary integral formulation. A three-dimensional formulation was developed for interacting deformable drops in Stokes flow which was applicable to very large deformations and problems with drops having cusped interfaces and drops closely

approaching break-up. Instead of the curvature, the formulation contained only the normal vectors, which are generally less sensitive to discretisation errors than the curvature. This allows simulation of problems including point and line singularities.

Khayat *et al.* [20] used a boundary element formulation to study two-dimensional two-phase incompressible creeping flow, applying the method to the deformation of a viscous drop inside a hyperbolic convergent channel in the absence of surface tension. The effect of changing the degree of channel convergence and the viscosity ratio, λ, were studied. It was found that the channel geometry significantly influenced drop deformation and that drop deformation increased with decreasing viscosity ratio, with particularly large extension when λ<1. Both initially circular and elliptical drops were considered.

Khayat *et al.* [21] later studied the deformation of single drops in two-dimensional convergent-divergent channel flows. Both Newtonian and viscoelastic fluids were considered. The effect of drop size, drop initial position relative both to the channel axis and the constriction throat, interfacial tension and fluid elasticity on the drop deformation were studied. Experimental results were also obtained and good agreement between computational and experimental results was seen. For drops initially positioned away from the channel axis, the distance from the axis was found to influence the rate and magnitude of drop deformation. In this case, the value of the viscosity ratio was found to be particularly important as, for drops with high viscosity ratios, little deformation was seen due to the drop rotating and being alternately stretched and compressed.

Giraldo *et al.* [22] recently studied the mobility problem of two particles in a shear flow for the complete range of viscous ratio, including bubbles, drops and solid particles. A completed indirect boundary integral equation formulation was used [4], and the motion of drops studied for different viscosity ratios and capillary numbers.

The present paper extends the above works of Khayat *et al.* [20, 21] by analysing the interaction between two drops. Appropriate numerical algorithms developed for this application with quadratic boundary elements are reported in the paper.

2. Integral Equation Formulation for Drop Deformation in Stokes Flow

Since the problem involves drops of a viscous fluid in another carrying fluid, a standard subregions technique is applied by considering compatibility and equilibrium conditions along the interfaces.

The relevant compatibility conditions at the interface between drop and bulk fluid are:

$$u_i^f(x) - u_i^d(x) = 0 \tag{1}$$

where u_i^f is the interface velocity of the bulk fluid and u_i^d is the velocity at the drop surface. This equation represents continuity of velocity.

The relevant equilibrium conditions are

$$t_i^f(x) - t_i^d(x) = \gamma\kappa(x)n_i(x) \tag{2}$$

where t_i is the traction, $t_i = \sigma_{ij}n_j$, γ is the surface tension coefficient, n_i is the unit outward normal vector and κ is the surface curvature. The difference between the tractions t_i^f and t_i^d is due to the existence of surface tension.

The velocity field for a point x' in Stokes flow can be written as [3, 4]

$$c_{ij}(x')u_j(x') = \frac{1}{\mu}\int_S u_{ij}^*(x',x)\,t_j(x)\,dS - \int_S p_{ij}^*(x',x)\,u_j(x)\,dS \tag{3}$$

where μ is the fluid viscosity, c_{ij} is the free term, and u_{ij}^* is the velocity field of the fundamental solution with traction p_{ij}^* [3, 4].

Since the BEM formulation in this paper is only concerned with the evolution of the drop boundary, and not with the calculation of the tractions on the drop boundary, it is possible to combine two integral equations, one for source points belonging to the bulk

fluid and the other for source points belonging to the drop, in order to eliminate the interface tractions by using the equilibrium equation (2) [20, 21], generating the following integral equations:.

$$c_{ij}(x')u_j(x') = \frac{1}{\mu_f}\int_{S_e} u_{ij}^*(x',x)t_j(x)\,dS - \int_{S_e} p_{ij}^*(x',x)u_j(x)\,dS + \frac{\gamma}{\mu_f}\int_{S_d} u_{ij}^*(x',x)\kappa(x)n_j(x)\,dS - (1-\lambda)\int_{S_d} p_{ij}^*(x',x)u_j(x)\,dS \quad (4)$$

for source points on the solid boundary, and

$$(1+\lambda)c_{ij}(x')u_j(x') = \frac{1}{\mu_f}\int_{S_e} u_{ij}^*(x',x)t_j(x)\,dS - \int_{S_e} p_{ij}^*(x',x)u_j(x)\,dS + \frac{\gamma}{\mu_f}\int_{S_d} u_{ij}^*(x',x)\kappa(x)n_j(x)\,dS - (1-\lambda)\int_{S_d} p_{ij}^*(x',x)u_j(x)\,dS \quad (5)$$

for source points on the drop. In the above equations, $\lambda = \frac{\mu_d}{\mu_f}$ is the viscosity ratio, with μ_f the bulk fluid viscosity and μ_d the drop viscosity, S_e and S_d represent the external and the drop boundary.

3. Numerical Algorithms

The numerical formulation employed quadratic boundary elements. Since small time steps are used in the simulation, the previous drop position and shape provide a very good initial guess for the iteration process at the next time step. Some of the specific algorithms adopted in the current implementation are briefly discussed below.

3.1 Mass Conservation

A measure of the accuracy of the numerical algorithms is mass conversation. For this, a simple application of the divergence theorem can be derived that allows the drop area at each time step to be calculated through the boundary integral

$$A = \frac{1}{2}\int_S x_i n_i dS \tag{6}$$

3.2 Node Relocation

Initially, elements on the drop surfaces are of equal size with evenly spaced nodes. After deformating the drop surfaces by translating nodes as if they were individual particles, there is no guarantee that the mid-element nodes will still be equidistant from each end node and, in addition, the elements will no longer be of equal size.

As is well known, the physical coordinates (x and y) that describe quadratic element geometries can be written as a function of a natural coordinate ξ, as follows:

$$x = \frac{1}{2}\xi(\xi-1)x_1 + (1-\xi)(1+\xi)x_2 + \frac{1}{2}\xi(\xi+1)x_3 \tag{7}$$

$$y = \frac{1}{2}\xi(\xi-1)y_1 + (1-\xi)(1+\xi)y_2 + \frac{1}{2}\xi(\xi+1)y_3 \tag{8}$$

where x_i and y_i stand for element node coordinates (see the sketch depicted in Figure 1). The mid-node location can be computed by evaluating the natural coordinate ξ_M corresponding to the physical mid-element position. In order to do so in a simple way, first, the horizontal and vertical centres of the element are computed ($X_M = [x_3 + x_1]/2$ and $Y_M = [y_3 + y_1]/2$) and, in the sequence, their respective natural coordinates (ξ_x and ξ_y) are evaluated by finding the roots of the following second-order equations:

$$(x_1 - 2x_2 + x_3)\xi_x^2 + (x_3 - x_1)\xi_x + 2(x_2 - X_M) = 0 \tag{9}$$

$$(y_1 - 2y_2 + y_3)\xi_y^2 + (y_3 - y_1)\xi_y + 2(y_2 - Y_M) = 0 \tag{10}$$

Once ξ_x and ξ_y are computed, ξ_M can be calculated by taking into account a simple weighted arithmetic mean,

$$\xi_M = \left(|\Delta X|\xi_x + |\Delta Y|\xi_y\right)/\left(|\Delta X| + |\Delta Y|\right) \tag{11}$$

and the new element mid-node location (coordinates *x* and *y*) can be obtained by applying the computed ξ_M into equations (7) and (8).

In the present work, at each time step, the above described procedures are employed three times: twice to relocate the element mid-nodes and once to relocate the element end-nodes. First, the mid-nodes of the quadratic elements are translated to their central positions (as discussed above); secondly, the above described procedures are employed to relocate the element end-nodes, fitting a quadratic curve between adjacent element mid-nodes and finding its central position; finally, considering the newly-dimensioned elements, the relocation procedures are once again applied to centre the element mid-nodes.

4. Numerical Simulations

The numerical simulations study initially circular drops placed in a converging channel and released, becoming instantaneously subject to the motion of the suspending fluid. The fluid in the channel flows due to a pressure difference between inlet and outlet. A sketch of the converging channel and drops (initial configuration), as well as some geometric parameters, is depicted in Figure 2. In all the numerical simulations discussed here, the circular drops are discretised by using 30 equal-sized quadratic boundary elements and the adopted time-step is $\Delta t = 0.04$ (in the present text, all units are omitted since any compatible unit system is valid).

In order to investigate the effect of a second drop on an initially centered drop, a parametric study is carried out by considering different initial relative positions of the drops, physical properties and geometric definitions. This initial study neglects surface tension, thus the capillary number *Ca* takes the value $Ca^{-1} = 0$ ($Ca = \mu_f v/\gamma$, with *v* a

characteristic velocity). Figure 3 depicts the evolution of the drops along a channel with L = 8.0 and converging ratio H_2/H_1 = 0.2, considering different physical properties for the first drop (initially centered drop) and different radii for the second drop. Snapshots are shown in Figure 3 for time intervals of 100Δt. The figure shows that, once the drops have entered the constriction, they take on an elongated shape due to elongational and shear effects. The results in Figures 3(a)-(b) (one drop analyses) are consistent with those of Khayat *et al*. [20, 21], obtained for different channel geometry but similar convergence and viscosity ratios. Results in Figures 3(c)-(h) illustrate how the interaction between the drops can increase or decrease, according to the geometrical and/or physical parameters involved. The presence of the second drop drastically influences the first drop flow in Figure 3(h), while no significant influence is observed in that flow due to the second drop presence in Figure 3(c).

Figure 4 shows the time evolution of the horizontal and vertical mass centre position of the initially centered drop, considering the different physical and geometrical parameters adopted. It can be observed that the horizontal velocity (tangent to the curve) of the initially centered drop is not drastically affected by the second drop, for the cases considered. The influence of the second drop on the symmetry of the model can be analyzed regarding the vertical mass centre evolution of the initially centered drop: as can clearly be observed in Figure 4, the larger the radius of the second drop, the more asymmetric the model becomes.

Figure 5 depicts boundary element discretisations for the deformed drop, at time 600Δt (one drop analysis – λ = 1.0), taking into account the proposed remeshing procedure and no remeshing. Figure 5(b) shows that there is a gradual decrease in the length of the elements approaching the drop ends, making the discretisation more refined in this region, when no remeshing procedures are considered. As is well known, this may cause numerical problems if elements become very small and nodes become too close, as the integrals required for the computations of the BEM matrices may become nearly singular. The boundary element discretisation depicted in Figure 5(a) highlights the effectiveness of the proposed remeshing technique, as approximately equal-sized elements (and equally-spaced nodes) are still observed in the BEM discretisation.

In order to further explore the interactions between two drops (one initially centered) flowing through a converging channel, several analyses are carried out next, fixing the radii of the drops ($r_1 = r_2 = 1.0$) and varying their relative positions and physical properties, as well as the channel convergence ratio. Considering the same physical properties for both drops, four cases are considered, namely: (i) Case 1: $Ca = 0.5$ and $\lambda = 0.5$; (ii) Case 2: $Ca = 0.5$ and $\lambda = 5.0$; (iii) Case 3: $Ca = 5.0$ and $\lambda = 0.5$; (iv) Case 4: $Ca = 5.0$ and $\lambda = 5.0$. The selected initial relative positions between the drops are given by $d_1 = 0.0$ or 2.0 and $d_2 = 2.2$ or 3.0 and the selected convergence ratios for the channel are given by $H_2/H_1 = 0.2$ or 0.4 (with L = 3.0, for both cases).

Figure 6 shows the evolution of the drops along a channel with converging ratio defined by $H_2/H_1 = 0.2$, considering $d_1 = 0.0$, $d_2 = 2.2$ and 3.0, and the four cases analysed with different physical properties of the drops. Figure 7 is analogous to Figure 6, considering $d_1 = 2.0$. Figures 8 and 9 are analogous to Figures 6 and 7, respectively, considering $H_2/H_1 = 0.4$. Once again, Figures 6-9 depict snapshots at time intervals of $100\Delta t$.

As expected, the results show that the addition of surface tension decreases drop deformation, forcing the drop back to a circular shape as can be seen in Figures 6-9, where drops are less elongated and their ends are less pointed. The viscosity ratio also influences the flow and drop interaction, and surface tension effects on drop deformation are more significant when the viscosity ratio is lower. Geometric aspects, such as different initial relative positions between the drops and different channel convergence ratios, also have a major influence on the results, as can be observed in the figures (in some analyses, the relative position of the drops in the constricted part of the channel completely changes, as for instance, in Figures 8(a) and 9(a) or Figures 9(a) and (b), where the leading drop within the constricted part of the channel is shifted). It should be noted that, in some simulations described in Figures 6-9, extreme physical and geometric configurations are being considered: for instance, in Figures 7(a) and (c), the deformed drops do not fit in the constricted part of the channel, and the evolution of the drops is not depicted for times greater than $300\Delta t$. In these cases, non-physical results may arise since the present formulation does not consider drop coalescence.

Figure 10 shows the relative deformation of the initially centered drop, evaluated as $\alpha(t) = [P(t) - P_0]/P_0$, where $P(t)$ is the drop perimeter at time $t = 400\Delta t$ and P_0 is the initial drop perimeter, for the simulations described in Figures 6-9. It can be observed that surface tension has a major influence on drop deformation, increasing drop deformation up to 2.9 times for some of the cases studied, followed by the channel convergence ratio, which increases drop deformation by up to 2.3 times. It is important to highlight that, in all the analyses considered here, mass conservation was monitored and the change in the drop area did not exceed 1.35%, illustrating the good accuracy and robustness of the numerical procedures adopted.

5. Conclusions

In this paper, the work of Khayat *et al.* [20, 21] has been extended to investigate the effect of drop interactions on drop deformation in two-dimensional Stokes flow in a converging channel. In real processes, the effects of these interactions will become more significant as the suspension becomes more concentrated. The number of drops, the viscosity ratio of the problem and the proximity of drops all affect the nature and importance of the drop interactions. However, some of the results are non-physical since the model does not consider drop coalescence.

Problems involving two drops were investigated, for different channel convergence, drop initial position, viscosity ratio and capillary number, in order to study the effect that drop interaction has on drop deformation. It was seen that, if the drops are initially placed close together, the results are significantly different from those seen in the equivalent single drop problem.

The numerical algorithms of the BEM formulation were found to be accurate and robust for the present simulations, with mass conservation to around 1% in all cases.

References

[1] Stokes, G.G., *Transactions of the Cambridge Philosophical Society*, **9,** 8, 1851.

[2] Clift, R., Grace, J.R. and Weber, M.E., *Bubbles, Drops and Particles,* Academic Press, London, 1978.

[3] Pozrikidis, C., *Boundary Integral and Singularity Methods for Linearized Viscous Flow*, Cambridge University Press, Cambridge, 1992.

[4] Power, H. and Wrobel, L.C., *Boundary Integral Methods in Fluid Mechanics*, Computational Mechanics Publications, Southampton, 1995.

[5] Weinbaum, S. and Ganatos, P., Numerical multipole and boundary integral equation techniques in Stokes flow, *Annu. Rev Fluid Mech*, **22**, 275-316, 1990.

[6] Tanzosh, J., Manga, M. and Stone, H.A., Boundary integral methods for viscous free-boundary problems: deformation of single and multiple fluid-fluid interfaces, *Boundary Element Technology VII*, 19-39, Computational Mechanics Publications, Southampton, 1992.

[7] Stone, H., Dynamics of drop deformation and breakup in viscous fluids, *Annu. Rev Fluid Mech*, **26**, 65-102, 1994.

[8] Briscoe, B.J., Lawrence, C.J. and Mietus, W.G.P., A review of immiscible fluid mixing, *Advances In Colloid And Interface Science*, **81**, 1-17, 1999.

[9] Manga, M. and Stone, H.A., Buoyancy-driven interactions between two deformable viscous drops, *J. Fluid Mechanics*, **259**, 647-683, 1993.

[10] Rallison, J.M.and Acrivos, A.A., A numerical study of the deformation and burst of a viscous drop in an extensional flow, *J. Fluid Mechanics,* **89**, 191-200, 1978.

[11] Manga, M. and Stone, H.A., Low Reynolds number motion of bubbles, drops and rigid spheres through fluid-fluid interfaces, *J. Fluid Mechanics*, **287**, 279-298, 1995.

[12] Manga, M., Stone, H.A., Collective hydrodynamics of deformable drops and bubbles in dilute low-Reynolds-number suspensions, *J. Fluid Mechanics,* **300**, 231-263, 1995.

[13] Pozrikidis, C., The buoyancy-driven motion of a train of viscous drops within a cylindrical tube, *J. Fluid Mechanics*, **237**, 627-648, 1992.

[14] Zhou, H. and Pozrikidis, C., The flow of suspensions in channels: single files of drops, *Phys. Fluids A*, **5**, 311-324, 1993.

[15] Zhou H. and Pozrikidis C., The Flow of ordered and random suspensions of two-dimensional drops in a channel, *J. Fluid Mechanics*, 255:103-127, 1993

[16] Li, X., Charles, R. and Pozrikidis, C., Simple shear flow of suspensions of liquid drops, *J. Fluid Mechanics*, **320**, 395-416, 1996.

[17] Loewenberger, M. and Hinch, E.J., Numerical simulations of a concentrated emulsion in shear flow, *J. Fluid Mechanics*, **321**, 395-419, 1996.

[18] Roumeliotis, J. and Fulford, G.R., Droplet interactions in creeping flow, *Computers & Fluids*, **29**, 435-450, 2000.

[19] Zinchenko, A.Z., Rother, M.A. and Davis, R.H., Cusping, capture, and breakup of interacting drops by a curvatureless boundary-integral algorithm, *J. Fluid Mechanics*, **391**, 249-292, 1999.

[20] Khayat R.E., Luciani A. and Utracki L.A., Boundary-element analysis of planar drop deformation in confined flow. Part 1. Newtonian fluids, *Eng. Anal. Bound. Elem.*, **19**, 279-289, 1997.

[21] Khayat R.E., Luciani A., Utracki L.A. Godbille F. and Picot J., Influence of shear and elongation on drop deformation in convergent-divergent flows*, International Journal of Multiphase Flow*, **26**, 17-44, 2000.

[22] M. Giraldo, H. Power and W.F. Florez, Mobility of a viscous Newtonian drop in shear Newtonian flow, *International Journal of Dynamic of Fluids*, **3**, 109-132, 2007.

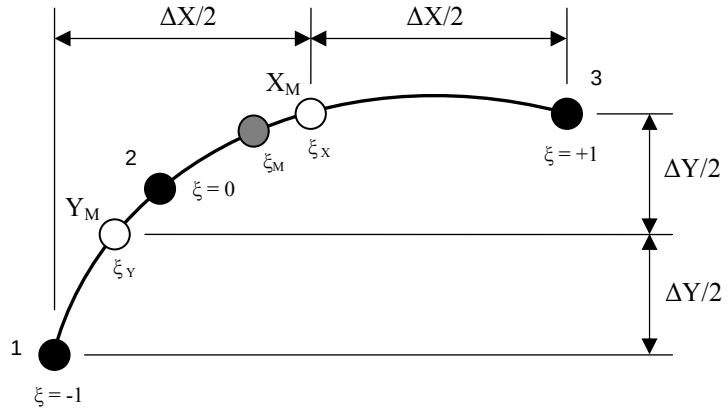

Figure 1 – Sketch for the element mid-node relocation procedure.

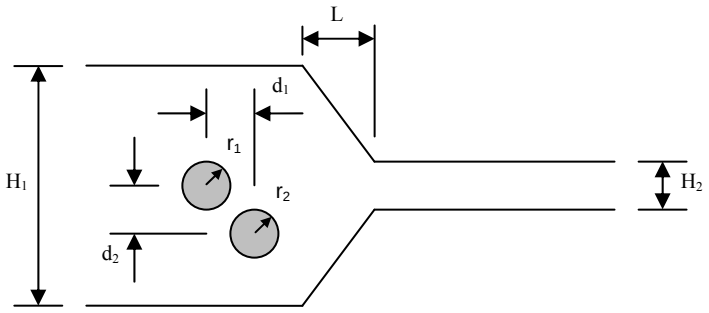

Figure 2 – Geometric (initial) configuration for the channel and drops

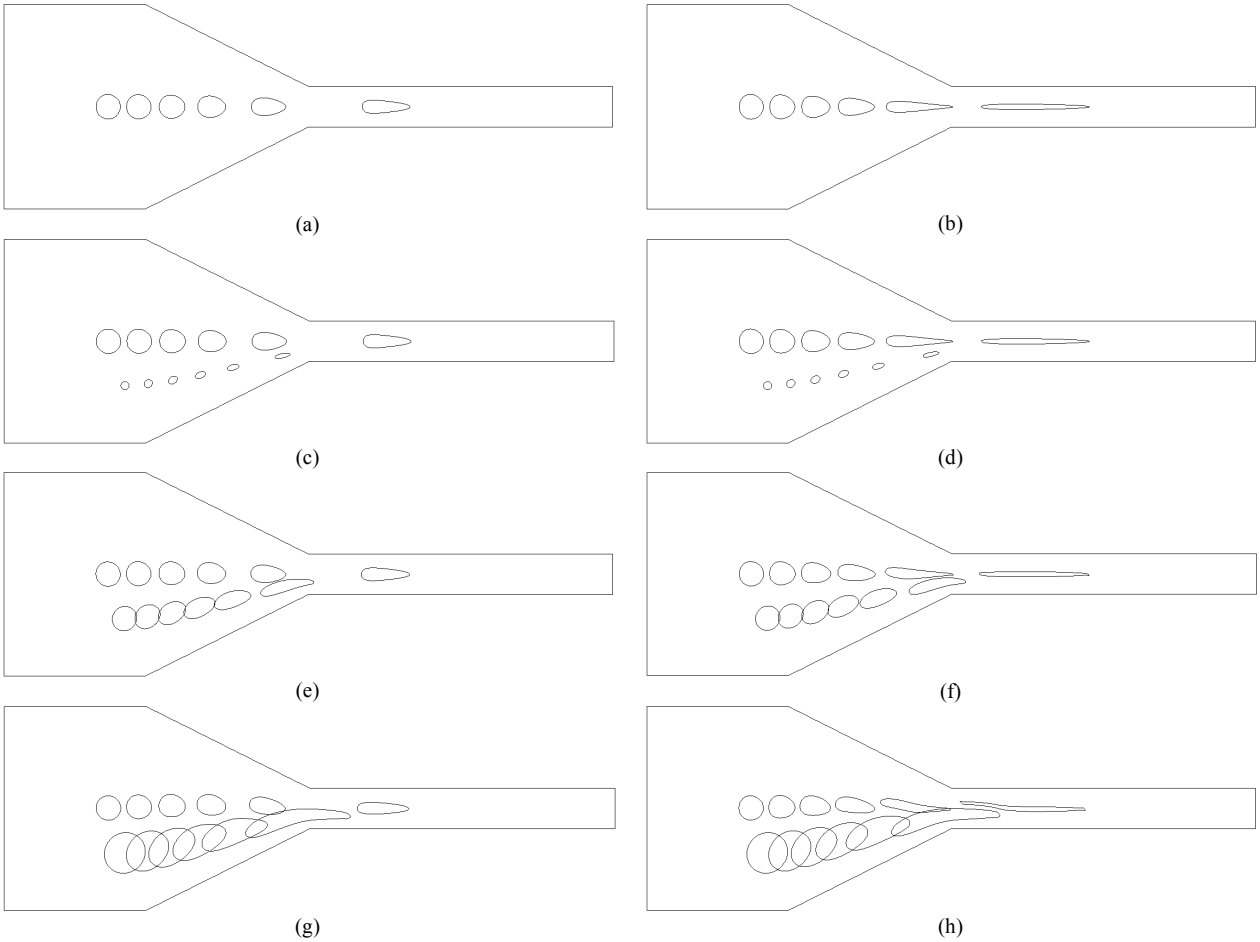

Figure 3 – Evolution of drops in channel with convergence ratio $H_2/H_1 = 0.2$ and $L = 8.0$ ($d_1 = 1.0$; $d_2 = 2.2$; $Ca^{-1} = 0$; $r_1 = 0.6$ and $\lambda_2 = 5.0$): (a) $\lambda_1 = 5.0$ and $r_2 = 0.0$; (b) $\lambda_1 = 1.0$ and $r_2 = 0.0$; (c) $\lambda_1 = 5.0$ and $r_2 = 0.2$; (d) $\lambda_1 = 1.0$ and $r_2 = 0.2$; (e) $\lambda_1 = 5.0$ and $r_2 = 0.6$; (f) $\lambda_1 = 1.0$ and $r_2 = 0.6$; (g) $\lambda_1 = 5.0$ and $r_2 = 1.0$; (h) $\lambda_1 = 1.0$ and $r_2 = 1.0$.

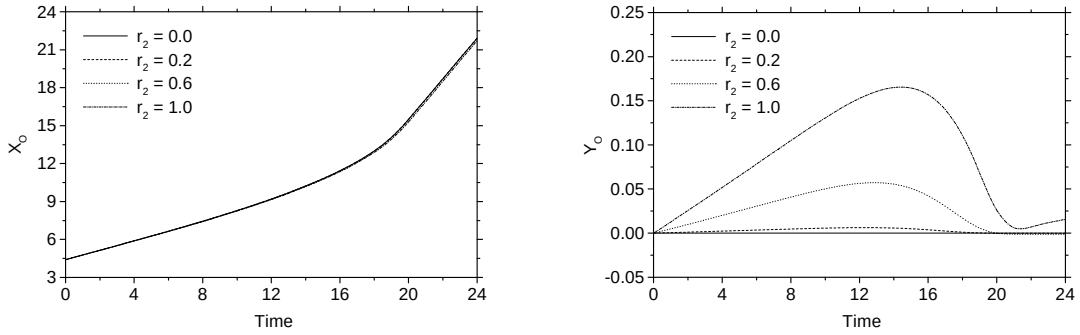

(a)

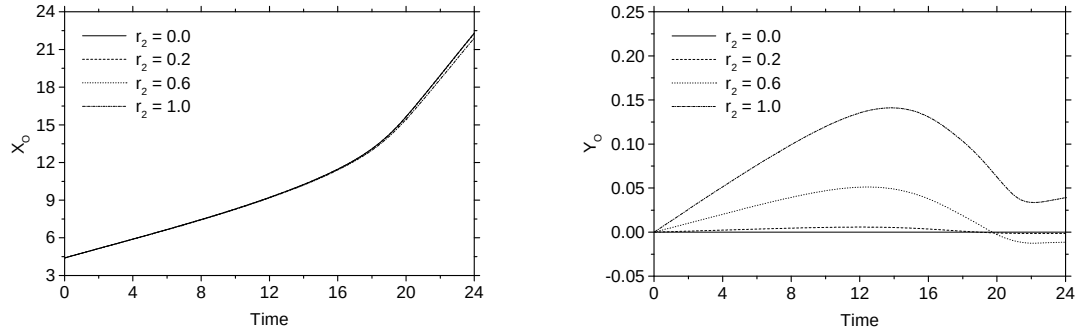

(b)

Figure 4 – Time evolution of the mass centre position (X_0 and Y_0) of the initially centered drop (see Figure 3): (a) $\lambda_1 = 5.0$; (b) $\lambda_1 = 1.0$.

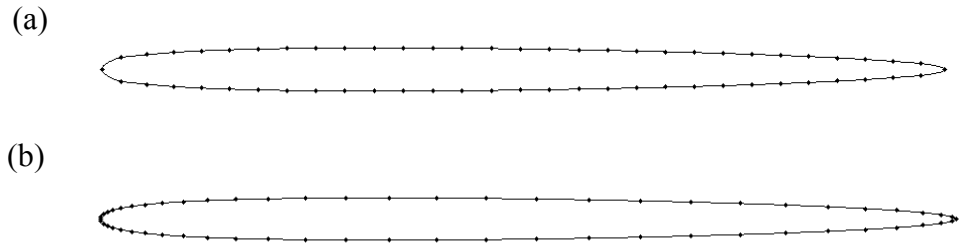

Figure 5 – Boundary element discretization for the drop, at time 600Δt (see Figure 3(b)): (a) considering remeshing procedures; (b) without remeshing.

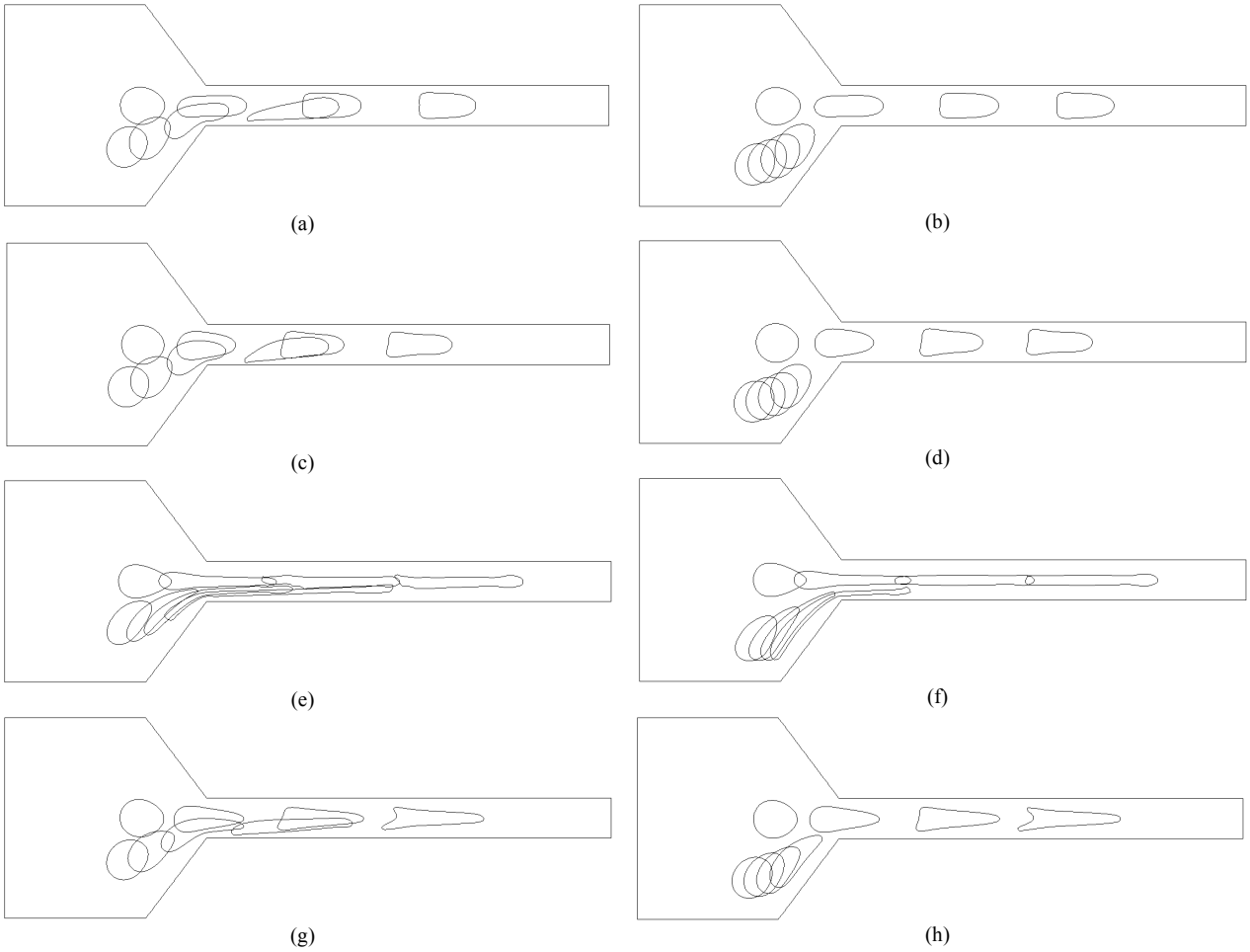

Figure 6 – Evolution of drops in channel with convergence ratio $H_2/H_1 = 0.2$ and $L = 3.0$ ($d_1 = 0.0$): (a) case 1 and $d_2 = 2.2$; (b) case 1 and $d_2 = 3.0$; (c) case 2 and $d_2 = 2.2$; (d) case 2 and $d_2 = 3.0$; (e) case 3 and $d_2 = 2.2$; (f) case 3 and $d_2 = 3.0$; (g) case 4 and $d_2 = 2.2$; (h) case 4 and $d_2 = 3.0$.

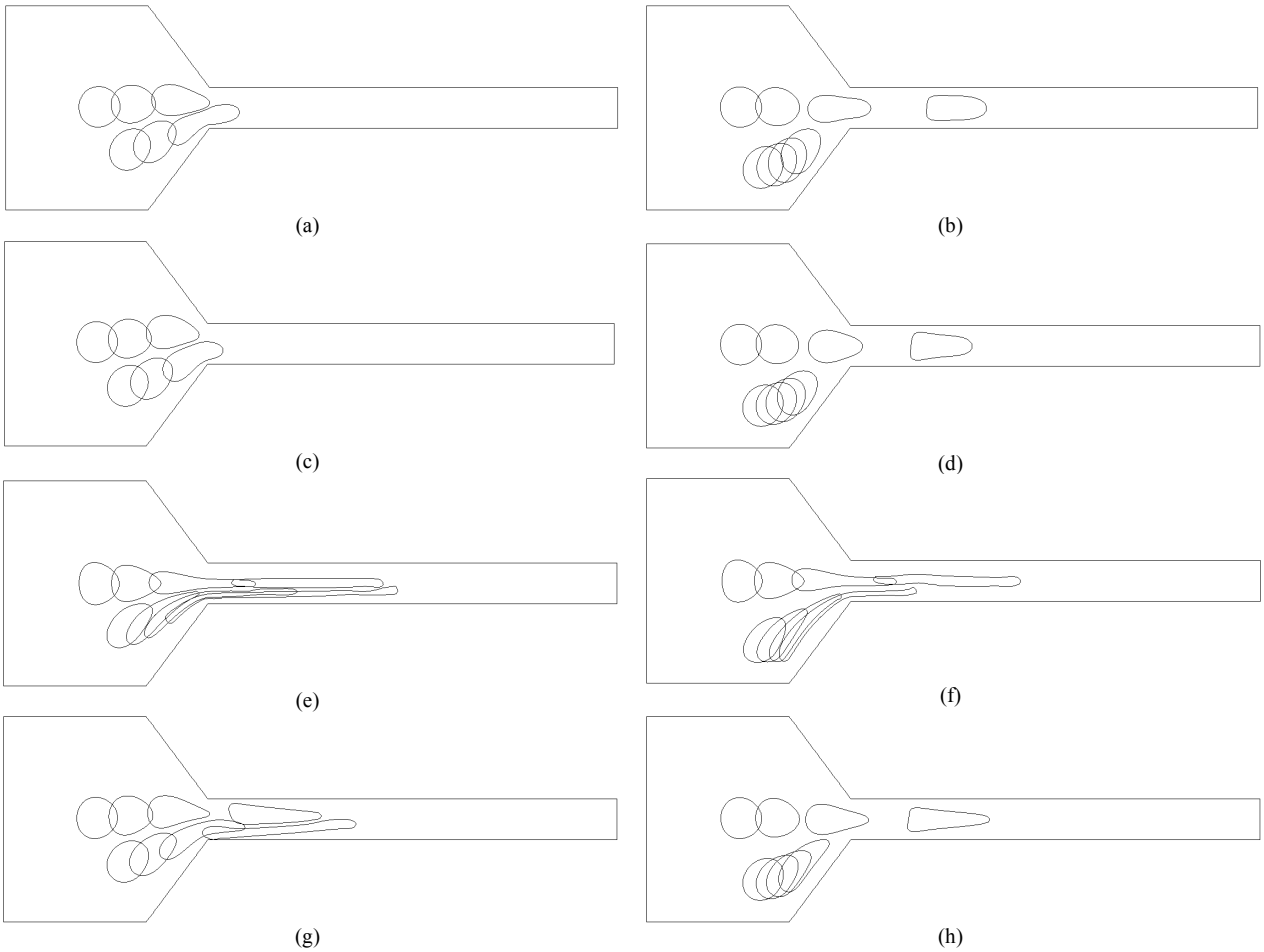

Figure 7 – Evolution of drops in channel with convergence ratio $H_2/H_1 = 0.2$ and $L = 3.0$ ($d_1 = 2.0$): (a) case 1 and $d_2 = 2.2$; (b) case 1 and $d_2 = 3.0$; (c) case 2 and $d_2 = 2.2$; (d) case 2 and $d_2 = 3.0$; (e) case 3 and $d_2 = 2.2$; (f) case 3 and $d_2 = 3.0$; (g) case 4 and $d_2 = 2.2$; (h) case 4 and $d_2 = 3.0$.

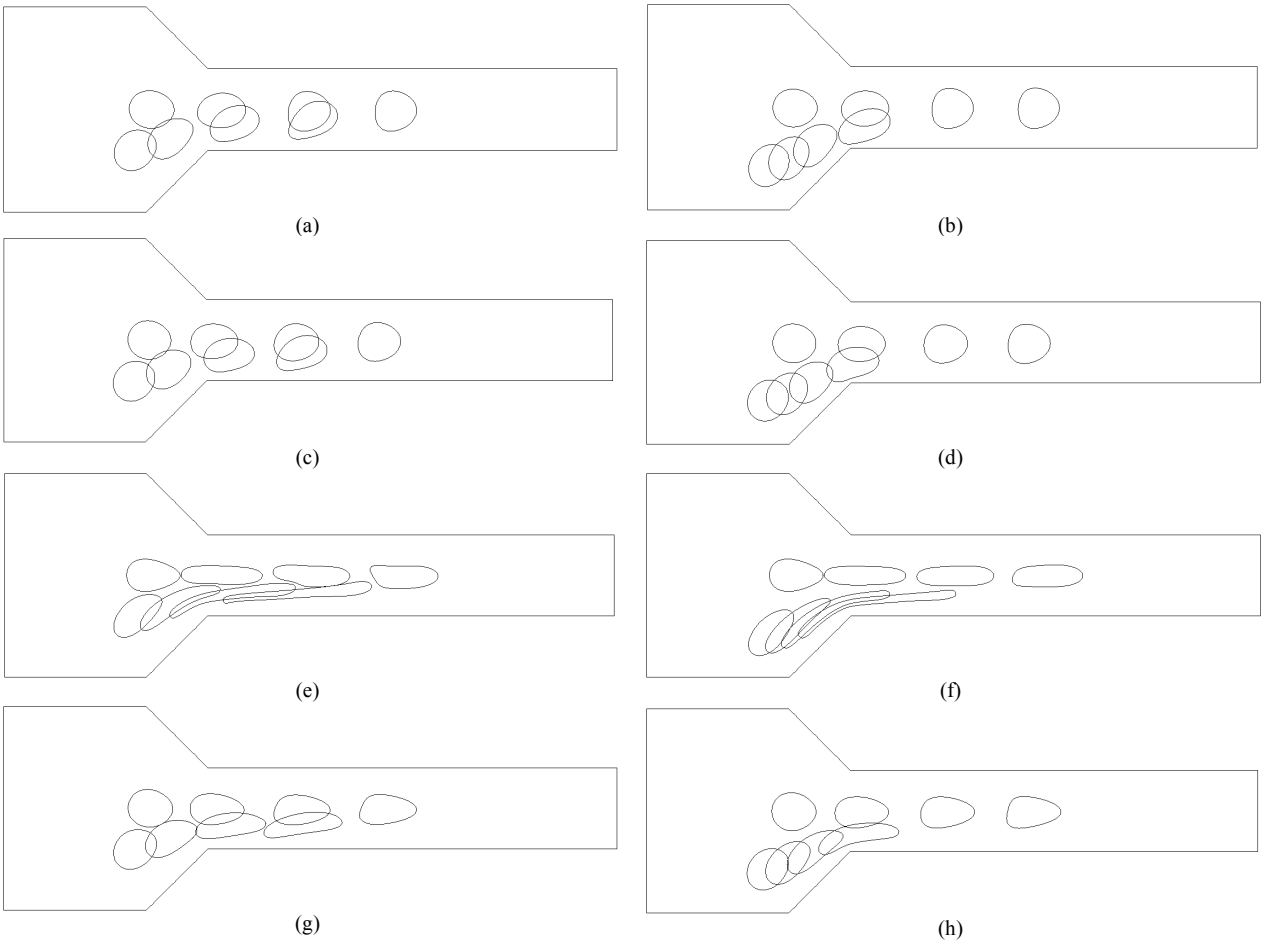

Figure 8 – Evolution of drops in channel with convergence ratio $H_2/H_1 = 0.4$ and $L = 3.0$ ($d_1 = 0.0$): (a) case 1 and $d_2 = 2.2$; (b) case 1 and $d_2 = 3.0$; (c) case 2 and $d_2 = 2.2$; (d) case 2 and $d_2 = 3.0$; (e) case 3 and $d_2 = 2.2$; (f) case 3 and $d_2 = 3.0$; (g) case 4 and $d_2 = 2.2$; (h) case 4 and $d_2 = 3.0$.

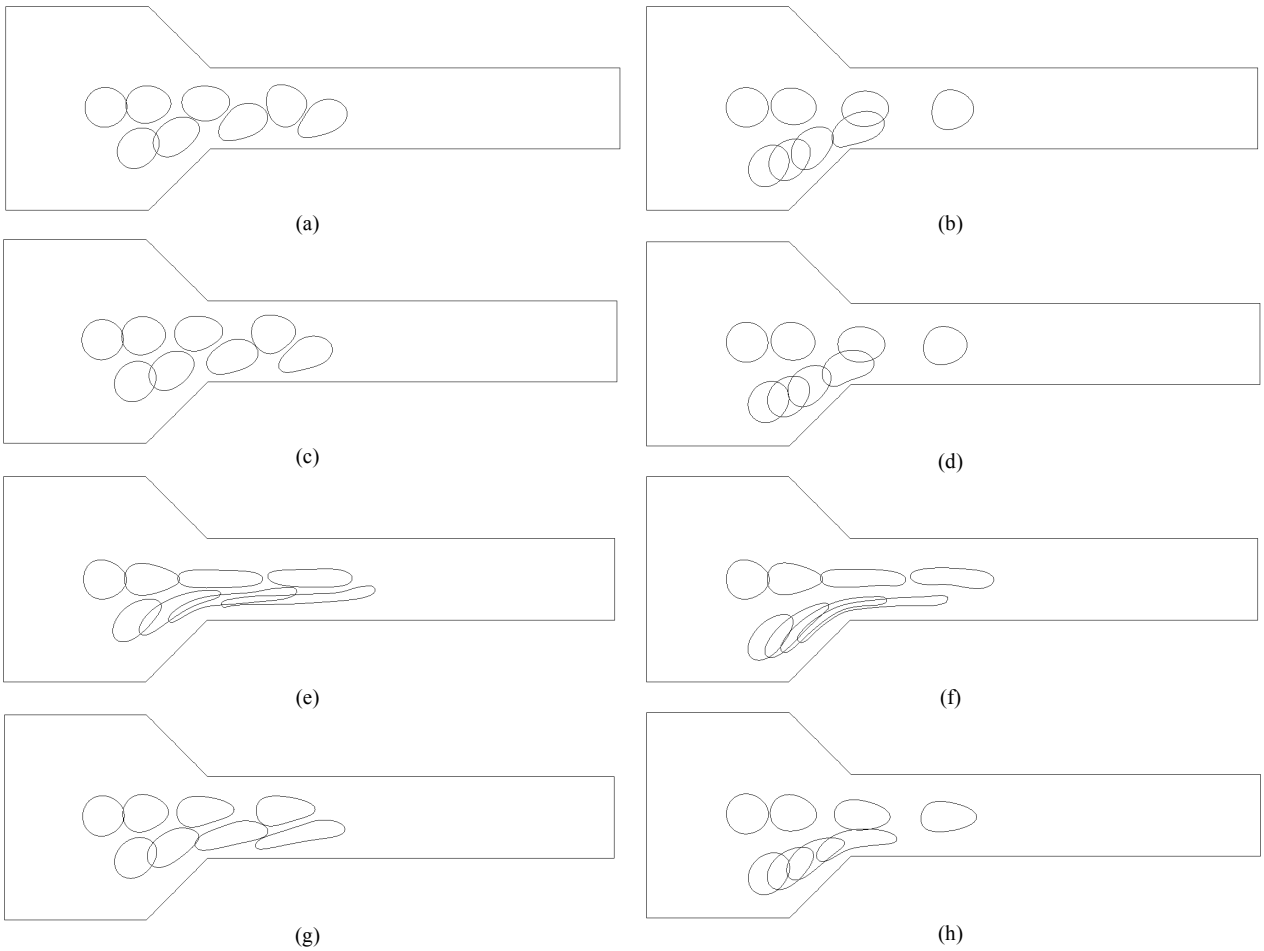

Figure 9 – Evolution of drops in channel with convergence ratio $H_2/H_1 = 0.4$ and L = 3.0 ($d_1 = 2.0$): (a) case 1 and $d_2 = 2.2$; (b) case 1 and $d_2 = 3.0$; (c) case 2 and $d_2 = 2.2$; (d) case 2 and $d_2 = 3.0$; (e) case 3 and $d_2 = 2.2$; (f) case 3 and $d_2 = 3.0$; (g) case 4 and $d_2 = 2.2$; (h) case 4 and $d_2 = 3.0$.

(a)

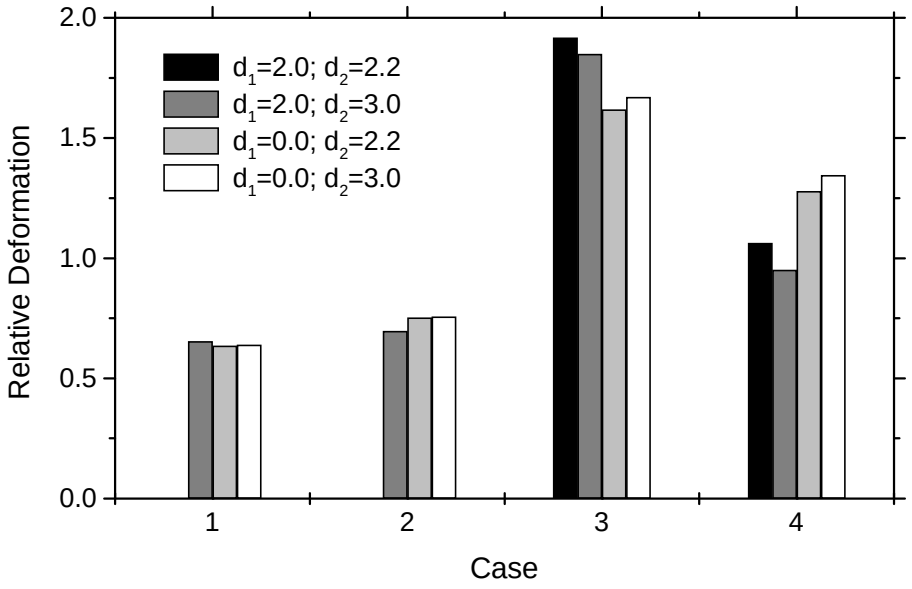

(b)

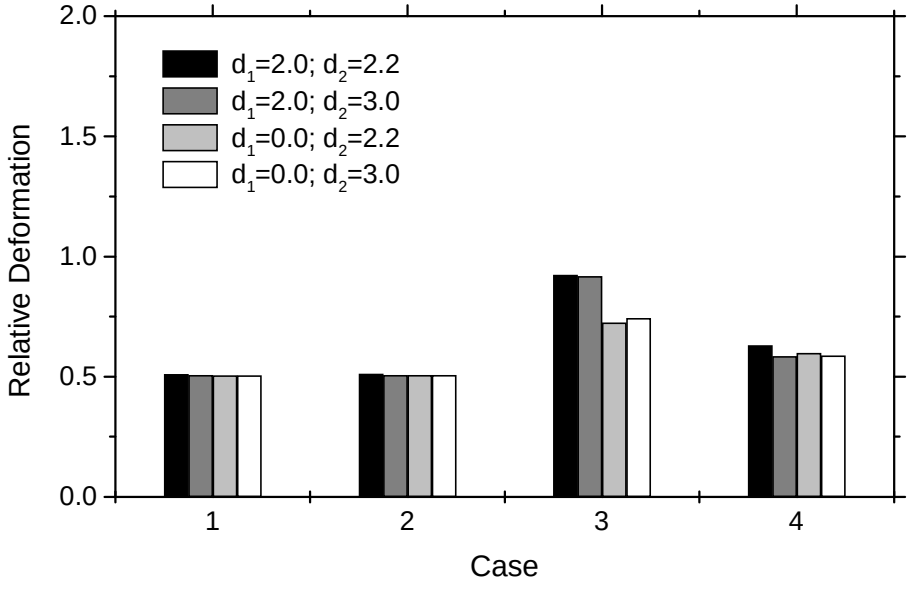

Figure 10 – Relative deformation of the initially centered drop at time 400Δt considering different relative positions (d_1 and d_2) and physical properties (Cases 1-4) for the drops: (a) $H_2/H_1 = 0.2$; (b) $H_2/H_1 = 0.4$.